Proceedings of the XIII International Conference "Ion Implantation and Other Applications of Ions and Electrons"

Modification of PET Foil by 150 keV Li^+ Ion Implantation

M. Turek*, A. Droździel, K. Pyszniak and W. Grudziński

Institute of Physics, Maria Curie Sklodowska University in Lublin, Pl. M. Curie-Skłodowskiej 1, 20-031 Lublin, Poland

Doi: 10.12693/APhysPolA.142.753 *e-mail: mturek@kft.umcs.lublin.pl

Very thin (3 μm in thickness) polyethylene terephthalate polymer foils were implanted with 150 keV Li^+ with fluences in the range from 1×10^{14} cm^{-2} up to 2×10^{16} cm^{-2}. Modification of the irradiated polymer microstructure was studied with the Fourier transform infrared spectroscopy and Raman spectroscopy. Breaking of a variety of chemical bonds followed by the formation of carbon clusters made of sp^2 C was proved. The dominance of the rings in the carbonized, graphite-like subsurface layer is demonstrated based on the fact that the *G* band prevails in the Raman spectra for larger Li^+ fluences. The rise of the absorbance within 200–800 nm is observed. Tauc's plots analysis enables the estimation of optical bandgap values that decrease from 3.95 eV (pristine polyethylene terephthalate) down to 1.4 eV (fluence of 2×10^{16} cm^{-2}). This change is not as dramatic as in the case of heavier projectiles like K^+ or Na^+. Reduction of surface resistivity by more than 2 orders of magnitude is observed in the case of the sample irradiated with the fluence 1×10^{16} cm^{-2}, and this effect is much smaller than that induced by the heavier projectile bombardment with the same fluence.

topics: polymers modification, ion implantation, polyethylene terephthalate (PET)

1. Introduction

The role that polymers play in everyday life has become more and more important over the decades as they attract the attention of scientists and engineers due to properties such as low cost, low density, durability, plasticity, etc. [1]. Synthetic plastic materials could be provided in a wide variety of forms, properties, and compositions [2], meeting the demand for new technologies. Nevertheless, these materials are characterized by some drawbacks, including poor chemical and mechanical resistance or, which is more important in the electronics industry, sometimes unstable electrical properties [3] combined usually with very high electrical resistance, which limits their applications in electronics severely. Ion implantation is a well-established technique that could be successfully used for the surface treatment of different materials, changing their properties at the depth from several nanometres up to micrometres, depending on the projectile mass and energy. Irradiation with different kinds of ions could lead to improvement of surface properties such as wear resistance, (micro)hardness, and wettability [4–9]. Ion implantation could also be a successful technique for increasing the biocompatibility of those synthetic materials [10–16] or changing their antimicrobial properties [17]. It should be mentioned here that not only classical ion implantation is employed for polymer modification, but plasma immersion [18–20] and laser-based techniques [21] are also becoming more and more common in this field. Other popular techniques that allow efficient treatment and modification of polymers are electron beams or gamma ray irradiations [22–27].

It is well known that the particle irradiation of polymers induces a variety of processes that result in the above-mentioned modification of surface properties [28]. These include bond breaking, chain scissions, cross-linking, intensive degassing, and consecutive carbonisation [29, 30]. The kinetic energy of particles impinging the target could be lost in two processes. The first one is the nuclear stopping, involving elastic collisions of the projectile with the target atoms. This stopping mechanism is typical of relatively heavier projectiles and a lower energy range. It is commonly assumed that bond breaking and the following chain scission resulting in polymer degradation is typical in the cases where this type of stopping is dominant. The second stopping mechanism, which prevails for swift and light projectiles, is inelastic electronic stopping, involving intensive electronic excitations and ionization, leading to the formation of free radicals and cross-linking in the polymer. It was demonstrated that strong electronic stopping results in intensive dehydrogenation of the subsurface layer of the polymer target, as well as in huge emission of gases, like hydrogen or CO and CO_2 (the last two in the case of oxygen-containing polymers [29, 31]), and carbonisation of the upper layer of the sample.

Over the years, a variety of irradiated polymers was investigated. There were studies on the modification of polyurethane (PU) by N^+ and Ar^+ [12, 13, 18], polystyrene by Ar^+ [32], polyethylene (PE) by, e.g., H^+, He^+, Ar^+, Xe^+, and Ti^+ [33–37], polyaryletheretherketone (PEEK) by N^+ [38–40], polycarbonate (PC) by Ar^+ and Cu^+ [41–43], poly(allyl diglycol carbonate) (CR-39) by Ar^+ and Au^+ [21, 44, 45], polymethylmethacrylate (PMMA) by Au^+, Ag^+, B^+, and C^+ [46–48]. Many reports concerning the modification of irradiated elastomers, e.g., acrylonitrile-butadiene rubber (NBR), ethylene propylene diene monomer (EPDM), and polytetrafluoroethylene (PTFE) irradiated by He^+ [49–53] were also delivered. Last but not least, much effort has gone into the investigations of implanted polyethylene terephthalate (PET) [54–62].

The modification of the latter synthetic polymer, known under brand names such as Mylar, Dacron, Terylene, or Lawsan, attracts the attention of scientists due to the widespread use of this highly transparent material in numerous fields of industry, e.g., packaging, production of magnetic tapes, photovoltaics base [63, 64] and other electronics [65], fibre production [66], concrete reinforcement [67, 68], etc.

One of the typical effects of PET modification by ion irradiation is the darkening of the initially transparent polymer, which could be seen with the naked eye even for the fluences of the order of 10^{14} cm^{-2}. The changes in absorption in the ultraviolet (UV) and visible light (VIS) regions are due to the increasing disorder and formation of a carbonaceous cluster, which results in the appearance of new energy levels and the narrowing of the energy gap. The formation of a carbon cluster and even vast networks of conducting graphite-like structures leads to another common modification of irradiated PET, namely the dramatic reduction of polymer resistivity by several orders of magnitude.

These effects were also observed in our previous papers, in which modification of PET with noble gases and alkaline metal ions was investigated. The reduction of optical bandgap to the values below 1 eV was reported, as well as that of resistivity by more than 9 orders of magnitude (the case of 50 keV Na^+ irradiation). Changes in the FTIR (Fourier transform infrared spectroscopy) spectra were in agreement with the SIMS-TOF (secondary ion mass spectrometry time-of-flight) results [69], suggesting that real ranges of Na^+ in PET could be much larger than those predicted by the SRIM (Stopping and Range of Ions in Matter) package.

The aim of the presented paper was to examine how the change of projectile to the lightest alkaline metal (and consequently, an increase of the role played by the electronic stopping) changes the influence of irradiation on the polymer molecular structure and some physical properties. One may suspect that in the case of a very light projectile, the thickness of the modified layer would be comparable to that of the sample, especially in light of the results presented in [69]. One may also suspect that the large changes in PET resistivity will be observed on the reverse (unimplanted) side of the sample as well, which was already reported for noble gases (135 keV He^+, Ne^+, and Ar^+) [70]. Modification of the microstructure of the implanted polymer is studied using the FTIR and Raman spectroscopies. Changes in PET absorption are investigated using UV-VIS (ultraviolet-visible) spectroscopy. An additional analysis using Tauc's plots also enables a determination of changes in the optical bandgap due to the structural modifications of the subsurface layer of implanted PET. The results of resistivity measurements are also shown and discussed in the paper for both sides of the irradiated samples.

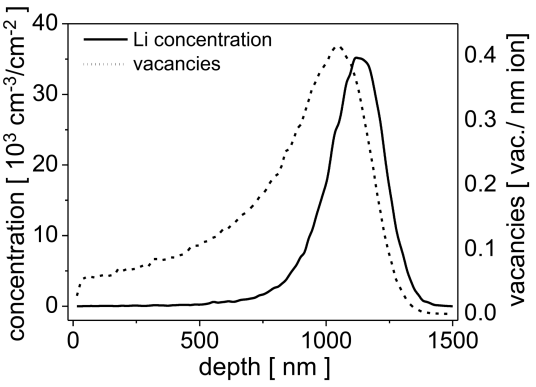

Fig. 1. Lithium atoms and vacancy depth profiles for the 150 keV Li^+ implantation calculated using the SRIM package.

2. Experimental

Very thin (3 μm, density $\simeq 1.4$ g/cm^3) PET polymer foils provided by Goodfellow were irradiated with 150 keV Li^+. The ion beam was produced using LiCl as a feeding substance and an arc discharge ion source with the internal evaporator described in [71,72]. Implantations were done with the fluences 10^{14} cm^{-2}, 10^{15} cm^{-2} , 5×10^{15} cm^{-2}, 10^{16} cm^{-2}, and 2×10^{16} cm^{-2}. Despite keeping the ion current density at a low level of 0.3 μA/cm^3 and placing the foil inside the ring holder, the most intensively irradiated sample was partially destroyed (shrunk), hence, e.g., resistivity measurements were not possible in that case.

The depth distribution of the dopant, as well as the vacancy density due to the irradiation, were estimated using the SRIM package [73]. The simulation results are presented in Fig. 1. The ion average range was $\simeq 1100$ nm, with 140 nm strangling. Having in mind the issues presented in [69] for the Na-implanted PET studied with SIMS-TOF, one has to be very cautious about the SRIM predictions as far

as the polymer targets are considered. The distribution of implanted Li atoms has a form of a relatively narrow peak, which is typical of the light projectile. However, based on the results presented in [69], one may expect that the real width of the modified layer is larger than that predicted by SRIM and comparable to the sample thickness.

Absorption spectra in the near UV and VIS regions were collected using the Cary 50 spectrometer (made by Agilent). The FTIR measurements were done employing the Nicolet iS50R (Thermo Scientific) spectrometer. Raman spectra were obtained using the Renishaw inVia system, with 514 nm excitation. The resistance of polymer samples (both virgin and modified) was measured using the Agilent B2911A measuring source and the set of polished electrodes of circular geometry.

3. Results and discussion

The changes in the polymer structure depend largely on the way the impinging projectile is stopped in the target. In the case of 150 keV Li^+, the dominant stopping mechanism is electronic stopping, i.e., in that case, the ratio of nuclear and electronic stopping powers, S_n/S_e, is 0.03. It is a matter of fact that the role played by the nuclear stopping increases while the projectile slows down; however, the total percentage of energy lost due to the electronic stopping is more than 92%, according to the detailed SRIM simulations. One may expect strong excitation and bond breaking, and as a consequence, e.g., a strong release of gases like hydrogen or oxygen. The destruction of chemical bonds in the irradiated samples is especially well visible in the FTIR spectra shown in Fig. 2 for C=O (stretching mode at $\simeq$ 1720 cm^{-1}), C–O (stretching at 1230 cm^{-1} and 1100 cm^{-1}), and C–H (bending mode also in the complex 1100 cm^{-1} peak) bonds. Similar behaviour is also observed for 730 cm^{-1} (out-of-plane C–H bending), 1018 cm^{-1} (in-plane C–H bending), 1340 cm^{-1} (CH_2 waggling mode), and other peaks. One can observe the reduction of the peak height by almost 50% in the case of the samples implanted with the fluence of 10^{16} cm^{-2} which could suggest that the heavily modified layer has a depth of 1.5 μm, which is slightly more than the SRIM estimated range of implantation. The decrease in the peak height is much more pronounced than in the previously considered cases of heavier alkali metals like Na^+ and K^+ [74, 75].

Structural changes in the irradiated polymer are also visible in the Raman spectra presented in Fig. 3. However, the evolution of these spectra with the implantation fluence is different from that observed in the case of heavier projectiles. Not only the most prominent peaks, i.e., these corresponding to C=O stretching (1727 cm^{-1}) and C=C in-ring stretching (1613 cm^{-1}), but also minor ones like C–C–C in-plane aromatic ring bending and breathing mode (857 cm^{-1}), C–O stretching (1097 cm^{-1}),

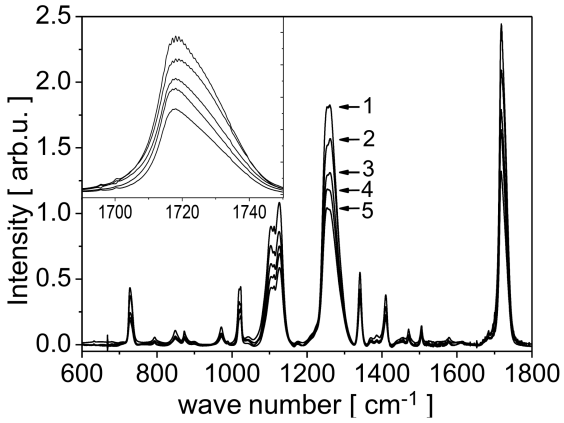

Fig. 2. FTIR spectra of the Li^+-implanted PET samples (1 — virgin PET, 2 — $\Phi = 10^{14}$ cm^{-2}, 3 — $\Phi = 10^{15}$ cm^{-2}, 4 — $\Phi = 10^{16}$ cm^{-2}, 5 — $\Phi = 10^{16}$ cm^{-2}).

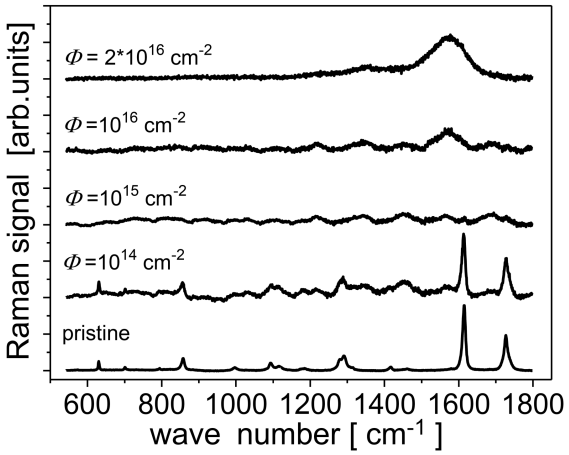

Fig. 3. Raman spectra for the samples implanted with different fluences of Li^+ ions.

C–H bending (1118 cm^{-1}), and complex mode — ring and O–C stretching (1286 cm^{-1}) — are well visible for the samples irradiated with 10^{14} cm^{-2}, while in the case of, e.g., K^+ irradiation, only the two strongest peaks survived. This is due to the above-mentioned fact that ion ranges are much larger in the case of Li^+ bombardment. Figure 1 suggests that most of the damage takes place at the relatively large depth of $\simeq$ 1 μm, at least for the low irradiation fluences, where the effects of dynamic target modification could be neglected. Moreover, Raman spectroscopy gives information about the microstructure at the surface layer, whose depth is of the order of the exciting light wavelength. Anyhow, a further increase of the implantation fluence (10^{14} cm^{-2}) makes all PET characteristic peaks disappear. It is worth noting that for even higher fluencies, the band centred at $\simeq$ 1580 cm^{-1} appears. For the most heavily modified samples, yet another lower band near 1350 cm^{-1} is also visible.

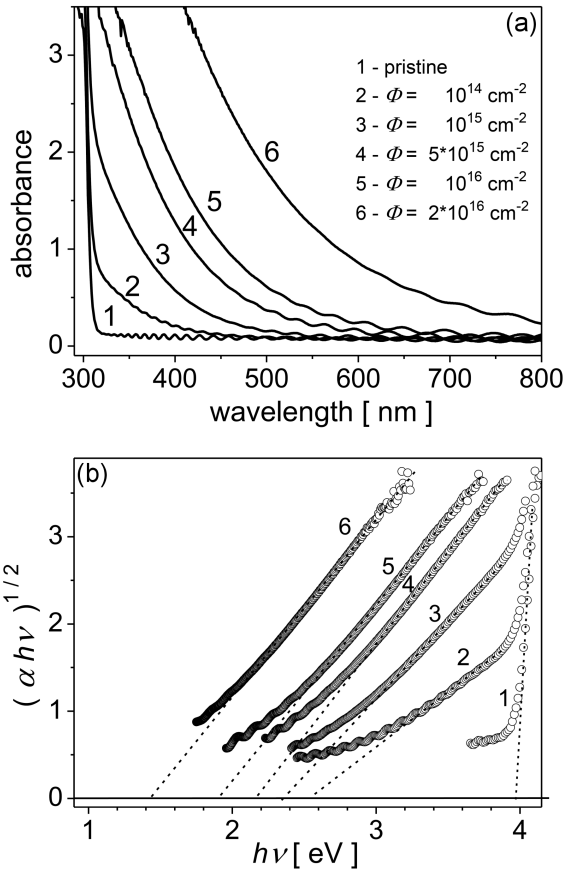

Fig. 4. UV-VIS absorbance spectra (a) and Tauc's plots (b) for the samples implanted with different Li^+ fluences.

These bands, usually referred to as G and D, are the signs of graphite-like structures made of sp^2 hybridised C atoms. The formation of vast graphite-like structures is a common feature of the implanted polymers [30, 31, 54–56]. This process is caused by both the chain scission during the elastic collisions within nuclear stopping and due to strong electronic excitations, leading to the breaking of the chemical bonds and the formation of free radicals. Both electronic and nuclear stopping mechanisms lead to intense degassing of the bombarded polymer and subsequent carbonization of the modified surface layer of that material. Graphite-like structures could be made by both chains and rings formed by the sp^2 C atoms. The Raman spectrum can provide some information concerning the relative concentration of these structures. The D band is a fingerprint of breathing modes typical of rings, while the G band is a sign of stretching modes that are typical of both rings and chains. One can notice that in the case of Li^+ irradiated PET, the formation of graphite-like structures is found in the Raman spectra for much (by order of magnitude) higher fluences than it was found for the Na or K projectiles. It is also worth noting that the D band is much lower than the G one, and the centroid of the latter matches almost perfectly the value 1582 cm^{-1}, which is obtained for pure graphite or graphene. The small ratio of D and G peaks heights (I_D/I_G) suggests that the Li bombardment induced the formation of rather well-organized carbon structures built mostly of rings, while the values close to 1, typical of heavier projectiles, point out to the emergence of more disordered graphite-like structures with a larger chain content [47]. Generally, it was observed that the content of disordered/chain-based structures in implanted PET increases with the mass of the projectile in the considered case.

TABLE I

Optical bandgap energies (E_o) estimated using the Tauc's approach, the average carbon cluster sizes (N), and Urbach energies (E_u) for different Li^+ irradiation fluences.

Φ [cm^{-2}]	E_o [eV]	N	E_u [eV]
0	3.96	–	0.055
1×10^{14}	2.55	181	0.67
1×10^{15}	2.35	213	0.78
5×10^{15}	2.15	255	0.93
1×10^{16}	1.90	326	1.42
2×10^{16}	1.40	600	1.19

The ion implantation induces a dramatic change in the light absorption by (initially) transparent polymers like PET. Darkening caused by the increased amount of the disorder due to carbonization could be seen with the naked eye. Indeed, this effect could be better described by performing measurements of, e.g., light absorption in the UV-VIS range. Some results for the range of 200–800 nm can be seen in Fig. 4a. The untreated sample is almost perfectly transparent for light of a wavelength larger than 310 nm. The formation of graphite-like structures, i.e., sp^2 carbon clusters, leads to the increase of light absorption as well as to the shift of the absorption edge towards larger wavelengths, as was observed for the heavier alkali metal projectiles like 150 keV Na^+ and K^+ [74, 75] as well as the inert gases (135 keV He^+, Ne^+ and Ar^+) [70]. Such effects as the decrease of the bandgap as a result of the emergence of new energy levels due to the formation of carbonaceous structures were observed for the other projectile-polymer target combinations [47, 48, 76]. However, it should be noticed that no signs of saturation of the absorption increase are observed in the considered fluence range, unlike in the case of heavier projectiles.

The bandgap (E_o) could be estimated using Tauc's approach. In the case of indirect allowed transition, one deals with an approximate relationship between the light energy $h\nu$ and the absorption coefficient

$$\alpha h\nu \simeq (h\nu - E_o)^2 . \quad (1)$$

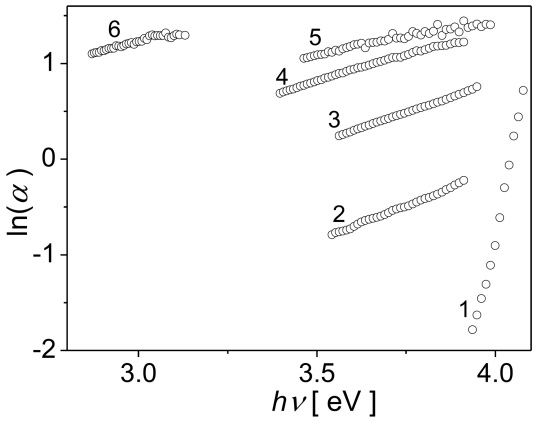

Fig. 5. Linear parts of $(\ln\alpha)$ vs $h\nu$ plots for the implanted PET samples (number description as in Fig. 4).

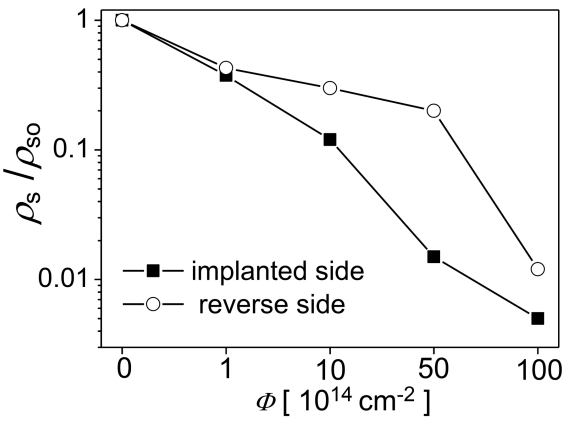

Fig. 6. Relative surface resistivity for the Li^+ implanted samples measured on both sides of foils.

The optical bandgap can be estimated by plotting $(\alpha h\nu)^{1/2}$ vs $h\nu$ and taking the interception of the linear part of the plot and the $h\nu$ axis. Such plots are shown in Fig. 4b. The calculated bandgap values are collected in Table I.

One can see the decrease of the bandgap from nearly 4 eV for the untreated PET to 1.4 eV for the most heavily modified sample. Nevertheless, the change is smaller than in the case of heavier projectiles, for which the E_o values below 1 eV were obtained (even up to 0.55 eV for 150 keV K^+ implanted PET with $\Phi = 10^{16}$ cm^{-2}). To sum up, the decrease of the bandgap due to the formation of vast carbon structures made of chains or rings is observed with increasing projectile mass.

The behaviour of absorption spectra in the case of ion-implanted polymer samples is, to a great extent, determined by the light absorption by the C clusters containing π-bonds. The change of the bandgap is strictly dependent on such bond concentration. There are several approaches that allow the estimation of the size of the carbon clusters based on the absorption data [77–79]. Following that discussed in [79], one can calculate the mean number of C atoms in a cluster (N) by

$$N = \left(\frac{34.3}{E_o\ [\mathrm{eV}]}\right)^2. \qquad (2)$$

The cluster sizes calculated for the Li-implanted PET samples are also presented in Table I. The mean size of the cluster increases with the fluences, like in all previously considered cases. However, the typical number of C atoms in the cluster for $\Phi = 10^{16}$ cm^{-2} ($N = 326$) is by an order of magnitude smaller than that estimated for the 150 keV K^+ and Na^+ implanted PET samples [74, 75].

The degree of disorder introduced into the polymer could be described by the Urbach energy E_u. This magnitude could be retrieved also from the optical absorption data by means of the Urbach edge method [80], as the subexponential absorption below the main (fundamental) absorption edge corresponds to the Urbach absorption edge. Such absorption could be approximated by the following relation

$$\alpha \simeq \exp\left[\frac{h\nu - E_p}{E_u}\right], \qquad (3)$$

where $h\nu$ is the photon energy, as previously, and E_p is a fitting parameter. Bearing this relation, in mind one can easily determine E_u as a reciprocal of the slope of the linear part of the $\ln(\alpha)$ vs $h\nu$ plot. Such plots for both irradiated and virgin PET samples are presented in Fig. 5.

The calculated Urbach energy values are gathered in Table I. As one can see, the disorder parameter E_u increases significantly from 0.055 eV up to $\simeq 1.4$ eV for the sample irradiated with the fluence of 10^{16} Li^+/cm^{-2}. For the most heavily modified sample, E_u is slightly smaller ($\simeq 1.2$ eV), which may be the result of measurement inaccuracy due to the fact that the sample is wrinkled, as mentioned above. The relatively large values of E_u could possibly be due to the large projected range of Li^+ in PET, leading to larger energy deposition and structural damage in deeper polymer layers [80].

Figure 6 presents the results of measurements of the relative (compared to the virgin PET) surface resistivity of the polymer as the function of the implantation fluence. As one may expect, the relative resistivity decreases with the fluence as a result of conducting graphite-like structures formation in the modified layer. However, this effect is not as spectacular for the light Li^+ projectiles as in the case of heavier ones [70, 74, 75]. One can see that the resistivity of the sample implanted with the fluence of 10^{16} Li^+/cm^{-2} is only $\simeq 2.5$ orders of magnitude smaller than that of the virgin sample. Again, this could be assigned to the large projected range of light Li^+ ions, leading to the formation of the most graphitised conducting layer buried beneath the relatively moderate modified (and therefore insulating) subsurface layer.

Moreover, the large projected range, combined with the fact that the thickness of the foil is of the same order (0.003 mm), causes the sheet resistivity on the reverse (non-implanted) side to be also significantly decreased as a result of irradiation. The sample resistivity on the reverse side implanted with the maximal fluence is 2 orders of magnitude smaller than that of the unmodified PET. A similar effect was observed also for the Na^+ irradiated samples [74], and this could be explained by the low thermal capacity of the very thin foil sample.

4. Conclusions

In the paper, the influence of 150 keV Li^+ irradiation (with fluences in the range of 10^{14} cm^{-2} up to 2×10^{16} cm^{-2}) on the microstructural, optical, and electrical properties of very thin PET foils is studied. The Raman and UV-VIS spectroscopy measurements confirmed the destruction of numerous bonds within the polymer, intensified with the irradiation fluence. Changes in the Raman spectra, namely the presence of broad D and G bands being the fingerprints of the amorphous graphite-like structures, point out the formation of carbon clusters made of C atoms with the orbitals in the sp^2 hybridisation. The fact that the D band is much less pronounced than the G one suggests that the graphite-like structures are built of carbon rings rather than chains, unlike the previously considered case of Na^+ or K^+ implantation. The evolution of absorbance spectra could also be understood as a consequence of the formation of carbon clusters and conducting structures in the modified layer. The reduction of the optical bandgap from its initial value (3.95 eV) down to 1.4 eV for the most heavily treated sample is observed, but this effect is not as strong as in the case of the heavier projectiles like K^+ or Na^+ (values close to 0.5 eV). Consequently, the average size of carbon clusters estimated from the bandgap is also smaller — reaching several hundreds of C atoms for $\Phi = 2 \times 10^{16}$ cm^{-2}. The ion irradiation introduces disorder to the polymer and results in the emergence of additional energy levels within the bandgap. The Urbach energy increases from 55 meV to $\simeq$ 1.2 eV in the case of the sample implanted with the fluence $\Phi = 2 \times 10^{16}$ cm^{-2}. The changes in the microstructure lead to the reduction of electrical sheet resistivity of the modified samples by, e.g., 2.5 orders of magnitude in the case of most heavily modified samples. The reduction of the resistivity is also observed on the non-implanted side of the foil. To sum up, the possibility of profound modification of numerous properties of PET polymer in the form of very thin foil via light projectile (like Li^+) irradiation has been successfully demonstrated.

References

[1] Y. Wu, T. Zhang, H. Zhang, X. Zhang, Z. Deng, G. Zhou, *Nucl. Instrum. Methods B* **169**, 89 (2000).

[2] M. Chawla, R. Rubi, R. Kumar, A. Sharma, S. Aggarwal, P. Kumar, D. Kanjilal, *Adv. Mater. Res.* **665**, 221 (2013).

[3] Y. Wu, T. Zhang, A. Liu, X. Zhang, G. Zhou *Sci. China E* **46**, 125 (2003).

[4] G.R. Rao, K. Monar, E.H. Lee, J.R. Treglio, *Surf. Coat. Technol.* **64**, 69 (1994).

[5] L. Torrisi, C. Gentile, A.M. Visco, N. Campo, *Radiat. Eff. Defects Solids* **158**, 731 (2003).

[6] M.J. Cook, J.H. Johnston, J. Leveneur, *Chem. Select* **3**, 5853 (2018).

[7] E.H. Lee, *Nucl. Instrum. Methods B* **151**, 29 (1999).

[8] N. Shekhawat, S. Aggarwal, A. Sharma, K.G.M. Nair, *J. Macromol. Sci. B* **55**, 652 (2016).

[9] Y. Kim, Y. Lee, S. Han, K.-J. Kim, *Surf. Coat. Technol.* **200**, 4763 (2006).

[10] M. Rahmati, E.A. Silva, J.E. Reseland, C.A. Heyward, H.J. Haugen, *Chem. Soc. Rev.* **49**, 5178 (2020).

[11] X. Cheng J. Fei A. Kondyurin, K. Fu, L. Yee, M.M. Bilek, S. Bao, *Mater. Sci. Eng. C* **99**, 863 (2019).

[12] A. Beliaev, A. Svistkov,. R. Iziumov, I. Osorgina, A. Kondyurin, M. Bilek, D. McKenzie, *IOP Conf. Ser. Mater. Sci. Eng.* **123**, 012001 (2016).

[13] I. Kondyurina, G.S. Nechitailo, A.L. Svistkov, A. Kondyurin, M. Bilek, *Nucl. Instrum. Methods B* **342**, 39 (2015).

[14] O. Nedela, P. Slepicka, V. Svorcík, *Materials* **10**, 1115 (2017).

[15] J. Jagielski, A. Piatkowska, P. Aubert, L.Thomé, A.Turos, A. Abdul Kader *Surf. Coat. Technol.* **200**, 6355 (2006).

[16] E. Sokullu, *Curr. Trends Biomed. Eng. Biosci.* **1**, 555567 (2017).

[17] H. Cao, X. Liu, F. Meng, P.K. Chu, *Biomaterials* **32**, 693 (2011).

[18] I.A.Morozov, A.S.Mamaev, I.V. Osorgina, L.M. Lemkina, V.P. Korobov, A.Y. Belyaev, S.E. Porozova, M.G. Sherban, *Mater. Sci. Eng. C* **62**, 242 (2016).

[19] E.A. Kosobrodova, A.V. Kondyurin, K. Fisher, W. Moeller, D.B. McKenzie, M.M. Bilek, *Nucl. Instrum. Methods B* **280**, 26 (2012).

[20] M.B. Tahir, M. Shahid Rafique, R. Ahmed, M. Rafique, T. Iqbal, A. Hasan, *Appl. Phys. B* **123**, 204 (2017).

[21] M.Z. Butt, D.A. Najm-ul-Aarifeen, S. Naseem, *Physica B Condens. Matter* **454**, 179 (2014).

[22] A.P. Tyutnev, V.S. Saenko, A.D. Zhadov, D.A. Abrameshin, *Polymers* **12**, 628 (2020).

[23] D. Manas, M. Bednarik, A. Mizera, M. Manas, M. Ovsik, P. Stoklasek, *Polymers* **11**, 1863 (2019).

[24] U. Gohs, R, Böhm, H. Brünig, D. Fischer, L. Häussler, M. Kirsten, M. Malanin, M.-T. Müller, C. Cherif, D.S.J. Wolz, H. Jäger, *Radiat. Phys. Chem.* **156**, 22 (2019).

[25] Z. Zimek, G. Przybytniak, A. Nowicki, *Radiat. Phys. Chem.* **81**, 1398 (2012).

[26] B. Nayak, S. Acharya, D. Bhattacharjee, R.I. Bakhtsingh, R. Rajan, D.K. Sharma, S. Dewangan, V. Sharma, R. Patel, R. Tiwari, S. Benarjee, S.K. Srivastava, *J. Instrum.* **11**, P03006 (2016).

[27] G. Przybytniak, E. M. Kornacka, K. Mirkowski, M. Walo, Z. Zimek, *Nukleonika* **53**, 89 (2008).

[28] D. V. Sviridov, in: *Chemical Problems of the Development of New Materials and Technologies*, Minsk 2003, p. 88

[29] M. Guenther, G. Gerlach, G. Suchaneck, K. Sahre, K.J. Eichhorn, B. Wolf, A. Deineka, L. Jastrabik, *Surf. Coat. Technol.* **158–159,** 108 (2002).

[30] V. Popok, *Rev. Adv. Mater. Sci.* **30**, 1 (2012).

[31] D.V. Sviridov, *Russ. Chem. Rev.* **74**, 315 (2002).

[32] M.M. Bilek, A. Kondyurin, S. Dekker, B. C. Steel, R. A. Wilhelm, R. Heller, D.R. McKenzie, A.S. Weiss, M. James, W. Möller *J. Phys. Chem. C* **119**, 16793 (2015).

[33] A. Turos, J. Jagielski, A. Piątkowska, D. Bieliński, L. Silusarski, N.K. Madi, *Vacuum* **70**, 201 (2003).

[34] N. Harrasser, S. Jüssen, I.J. Banke, R. Kmeth, R. von Eisenhart-Rothe, B. Stritzker, H. Gollwitzer, R. Burgkart, *AMB Express* **5**, 64 (2015).

[35] A. Valenza, A.M. Visco, L. Torrisi, N. Campo, *Polymer* **45**, 1707 (2004).

[36] M. Nenadović, J. Potocnik, M. Ristić, S. Strbac, Z. Rakocević, *Surf. Coat. Technol.* **206**, 4242 (2012).

[37] M. Abdul-Kader, A. Turos, D. Grambole, J. Jagielski, A. Piątkowska, N.K. Madi, M. Al-Maadeed, *Nucl. Instrum. Methods B* **240**, 152 (2005).

[38] E.A. Wakelin, A. Fathi, M. Kracica, G.C. Yeo, S.G. Wise, A.S. Weiss, D.G. McCulloch, F. Dehghani, D.R. Mckenzie, M.M. Bilek, *ACS Appl. Mater. Interfaces* **7**, 23029 (2015).

[39] K. Gan, H. Liu, L Jiang, X. Liu, X. Song, D Niu, T. Chen, C. Liu, *Dent. Mater.* **32**, e263 (2016).

[40] F. Awaja, D.V. Bax, S. Zhang, N. James, D.R. McKenzie *Plasma Processes Polym.* **9**, 355 (2012).

[41] P.K. Goyal, V. Kumar, Renu Gupta, S. Kumar, P. Kumar, D. Kanjilal *AIP Conf. Proc.* **1349**, 543 (2011).

[42] V. Resta, L. Calcagnile, G. Quarta, L. Maruccio, A. Cola, I. Farella, G. Giancane, L. Valli, *Nucl. Instrum. Methods Phys. Res. B* **312**, 42 (2013).

[43] V. Resta, G. Quarta, L. Maruccio, L. Calcagnile, *Nucl. Instrum. Methods Phys. Res. B* **331**, 187 (2014).

[44] N. Shekhawat, *Adv. Mater. Res.* **665**, 214 (2013).

[45] R. Sagheer, M. Shahid Rafique, F. Saleemi, S. Arif, F. Naab, O. Toader, A. Mahmood, R. Rashid, I. Hussain, *Mater. Sci. Pol.* **34**, 468 (2016).

[46] M.C. Salvadori, M. Cattani, F.S. Teixeira, I.G. Brown, *Appl. Phys. Lett.* **93**, 073102 (2008).

[47] T. Kavetskyy, K. Iida, Y. Nagashima, A. Kuczumow, O. Šauša, V. Nuzhdin, V. Valeev, A.L. Stepanov, *J. Phys. Conf. Ser.* **791**, 012028 (2017).

[48] S. Arif, M.S. Rafique, F. Saleemi, R. Sagheer, F. Naab, O. Toader, A. Mahmood, R. Rashid, M. Mahmood, *Nucl. Instrum. Methods Phys. Res. B* **358**, 236 (2015).

[49] A. Kosinska, J. Jagielski, U. Ostaszewska, E. Wyszkowska, M. Clozel, L. Kurpaska M.Romaniec, *Nucl. Instrum. Methods Phys. Res. B* **443**, 15 (2019).

[50] A. Kosinska, J. Jagielskia, E. Wyszkowska, M. Clozel, L. Kurpaska, J. Zagorski, B. Staszkiewicz, K. Gniadek, D. Bielinski, *Nucl. Instrum. Methods Phys. Res. B* **473**, 6 (2020).

[51] J. Jagielski, D. Grambole, I. Jozwik, D.M. Bielinski, U. Ostaszewska, D. Pieczynska, *Mater. Chem. Phys.* **127** 342 (2011).

[52] J. Jagielski, U. Ostaszewska, D. Bielinski, A. Piatkowska, M. Romaniec, *Acta Phys. Pol. A* **123**, 888 (2013).

[53] X. Zhou, X. Chen, T.C. Mao, X. Li, X.H. Shi, D.L. Fan, Y.M. Zhang, P*Last Reconstr. Surg.* **137**, 690e (2016).

[54] M. Djebara, J.P. Stoquert, M. Abdesselam, D. Muller, A.C. Chami, *Nucl. Instrum. Methods Phys. Res. B* **274**, 70 (2012).

[55] P.K. Goyal, V. Kumar, R. Gupta, S. Mahendia, S. Kumar, *Adv. Appl. Sci. Res.* **2**, 77 (2011).

[56] R. Kumar, M. Goyal, A. Sharma, S. Aggarwal, A. Sharma, D. Kanjilal *AIP Conf. Proc.* **1661**, 110010-1 (2015).

[57] M. Chawla, R. Rubi, R. Kumar, A. Sharma, S. Aggarwal, P. Kumar, D. Kanjilal, *Adv. Mater. Res.* **665**, 221 (2013).

[58] A. Tóth, M. Veres, K. Kereszturi, M. Mohai, I. Bertóti, J. Szépvölgyi, *Appl. Surf. Sci.* **257**, 10815 (2011).

[59] M.G. Lukashevich, V.N. Popok, V.S. Volobuev, A.A. Melnikov, R.I. Khaibullin, V.V. Bazarov, A. Wieck, V.B. Odzhaev, *The Open Appl. Phys. J.* **2**, 1 (2009).

[60] Yu.A. Bumai, V.S. Volobuev, F. Valeev, N.I. Dolgikh, M.G. Lukashevich, R.I. Khaibullin, V.I. Nuzhdin, V.B. Odzhaev, *J. Appl. Spectrosc.* **79**, 773 (2012).

[61] P. Malinsky, A. Mackova, V. Hnatowicz, R.I. Khaibullin, V.F. Valeev, P. Slepicka, V. Svorcik, M. Slouf, V. Perina, *Nucl. Instrum. Methods Phys. Res. B* **272**, 396 (2012).

[62] P.L. Sant'Ana, J. R. Ribeiro, N.C. da Cruz et al., *Nanomed. Nanotechnol. Open Access* **3**, 1 (2018).

[63] C.S. Goh, S.C. Tan, S.L. Ngoh, J. Wei, *Energy Procedia* **15**, 428 (2012).

[64] Y. Park, J. Berger, Zh. Tang, L. Müller-Meskamp, A.F. Lasagni, K. Vandewal, K. Leo, *Appl. Phys. Lett.* **109**, 093301 (2016).

[65] L. Frisk, S. Lahokallio, J. Kiilunen, K. Saarinen-Pulli, *MRS Adv.* **1**, 3477 (2016).

[66] *Handbook of Fiber Science and Technology Volume 2: Chemical Processing of Fibers and Fabrics*, Ed. M. Lewin, Routledge, 2018.

[67] J.M. Irwan, S.K. Faisal, N. Othman, I. Mohamad, H. Wan, R.M. Asyraf, M.M.K. Annas, *Adv. Mater. Res.* **795**, 352 (2013).

[68] N.F.A. Ahmad, S.N.M. Razali, S. Sahat, M. Kaamin, *AIP Conf. Proc.* **2016**, 020015 (2018).

[69] Yu Kudriavtsev, A.G. Hernández, R. Asomoza, V.M. Korol, *Surf. Interface Anal.* **49**, 1049 (2017).

[70] A. Droździel, M. Turek, K. Pyszniak, S. Prucnal, R. Luchowski, W. Grudziński, A. Klimek-Turek, J. Partyka, *Acta Phys. Pol. A* **132**, 264 (2017).

[71] M. Turek, A. Droździel, K. Pyszniak, S. Prucnal, *Nucl. Instrum. Methods Phys. Res. B* **269**, 700 (2011).

[72] M. Turek, A. Drozdziel, K. Pyszniak, S. Prucnal, J. Zuk, *Przeglad Elektrotechniczny* **86**, 193 (2010).

[73] J.F. Ziegler, M.D. Ziegler, J.P. Biersack, *Nucl. Instrum. Methods Phys. Res. B* **268**, 1818 (2010).

[74] M. Turek, A. Droździel, K. Pyszniak, R. Luchowski, W. Grudziński, A. Klimek-Turek. *Acta Phys. Pol. A* **136**, 278 (2019).

[75] M. Turek, A. Droździel, K. Pyszniak, W. Grudziński, A. Klimek-Turek, *Przegląd Elektrotechniczny* **96**, 151 (2020).

[76] V. Kumar, R.G. Sonkawade, S.K. Chakarvarti, P. Singh, A.S. Dhaliwal, *Radiat. Phys. Chem.* **81**, 65 (2012).

[77] I.P. Kozlov, V.B. Odzhaev, I.A. Karpovich, V.N. Popok, D.V. Sviridov, *J. Appl. Spectrosc.* **65**, 390 (1998).

[78] S.A. Nouh, M.H. Abdul-Salem, A. Ahmed Morsy, *Radiat. Meas.* **37**, 25 (2003).

[79] S. Gupta, D. Choudhary, A. Sarma, *J. Polym. Sci. B Polym. Phys.* **38**, 1589 (2000).

[80] M. Goyal, S. Aggarwal, A. Sharma, *J. Appl. Phys.* **119**, 115303 (2016).